J. Phase Equilib. Diffus.
https://doi.org/10.1007/s11669-023-01080-w

ORIGINAL RESEARCH ARTICLE

Study of Interface-Related Mechanisms in the Early Stage Precipitation of σ Phase in Hyper Duplex Stainless Steels

Aurélie Jacob[1] · Roman Schuster[1] · Laszlo Solyom[1] · Andreas Keplinger[2] · Erwin Povoden-Karadeniz[1,3]

Submitted: 25 September 2023 / in revised form: 10 November 2023 / Accepted: 1 December 2023

Abstract This work aims to computationally explore the diffuse prerequisites for σ phase precipitation in high-alloyed duplex steels. The diffusion control for the early precipitation stage of the σ phase was studied by the Calphad thermodynamic modeling combined with the DICTRA software. Different nucleation sites, α/γ, and α/α and γ/γ grain-boundaries, were studied using thermodynamic and mobility databases developed by the present authors in previous works for high-alloyed duplex stainless steel. Simulation results were compared to experimentally obtained microstructures of aged samples. The study of the concentration profiles of the elements Cr, Mo, and Ni revealed that the precipitation is most favorable within the α phase due to fast mobility and strong thermodynamic driving force favoring the formation of the σ phase. Based on the present results, the role of the different heterogeneous sites for the precipitation of the σ phase in hyper duplex steel is discussed.

This invited article is part of a special tribute issue of the *Journal of Phase Equilibria and Diffusion* dedicated to the memory of Thaddeus B. "Ted" Massalski. The issue was organized by David E. Laughlin, Carnegie Mellon University; John H. Perepezko, University of Wisconsin–Madison; Wei Xiong, University of Pittsburgh; and *JPED* Editor-in-Chief Ursula Kattner, National Institute of Standards and Technology (NIST).

✉ Aurélie Jacob
aurelie.jacob@tuwien.ac.at

[1] Christian Doppler Laboratory Interfaces Precipitation Engineering, Institute of Materials Science and Technology, TU Wien, Vienna, Austria

[2] voestalpine BÖHLER Edelstahl GmbH & Co KG, Kapfenberg, Austria

[3] Institute of Materials Science and Technology, TU Wien, Vienna, Austria

Keywords σ Phase · diffusion controlled · hyper duplex · moving boundary

1 Introduction

Due to their microstructural balance between ferrite and austenite and the high amount of Cr and Mo, duplex stainless steels possess excellent corrosion resistance and mechanical properties. By increasing the amount of alloying elements super duplex stainless steels were developed and are often replacing ferritic stainless steels or Ni-based alloys due to their lower cost. Following the trend of increased alloying, hyper duplex stainless steels (HDSS) comprising about 27 Cr, 7 Ni, 5 Mo, and 0.4 N (in wt.%) were developed. The hyper duplex steels have shown better corrosion resistance and higher strength compared to conventional duplex steels.[1] However, due to the high number of alloying elements, hyper duplex steel is prone to precipitation of detrimental intermetallic phases, such as σ phase, a complex Fe-Cr based intermetallic phase with tetragonal crystal structure, space group $P4_2/mnm$. Precipitation kinetics of σ phase in HDSS have been studied by the present authors[2] by Mean-Field approach based on the assessed thermodynamic database for high-alloyed steels.[3,4] Simulation and ex-situ[5,6] and in-situ aging experiments[7] showed that the kinetics of σ phase in HDSS is very fast, only a few seconds of aging around the nose temperature of time–temperature transformation (TTT) diagrams are needed to observe σ phase formation. Thus, in order to characterize and eventually better control the precipitation of σ phase, the early stage precipitation of σ phase should be better understood.

Published online: 19 December 2023

The aim of this paper is to clarify the diffusive prerequisites of σ phase nucleation, including moving boundaries between the steel matrix phases ferrite (α) and austenite (γ), and element partitioning. For this purpose, we compare the results of moving boundary simulation using DICTRA[8] (Diffusion ConTrolled Reaction module of Thermo-Calc) with microstructural results from Scanning Electron Microscopy (SEM) and chemical characterization by Energy Dispersive x-ray (EDX) measurements of isothermally aged samples in order to understand interface hierarchies for the heterogeneous precipitation of σ phase[9] at the interfaces between α/γ, α/α, and γ/γ.

2 Literature Review

The kinetics of σ phase precipitation has been studied experimentally for duplex,[10] super duplex,[6,11] and hyper duplex steels[5] . While the Zhang et al.[5] show a rather fast formation, i.e. after around 100 s at the nose temperature (T = 950 °C) from annealed and quenched samples, Schuster et al.[7] found by in-situ high energy x-ray diffraction (XRD) measurements that the precipitation of σ phase is even faster than stated by[5] being below 10 s at T = 900 °C (at even slightly lower alloying content of σ phase forming elements). In a more recent study than,[5] Zhang et al.[12] proposed adding more N in the alloy to slow down the kinetics of σ phase. However, adding N promotes the formation of Cr_2N which is also quite detrimental for the material and is thus not a suitable approach to reduce σ phase formation. The element distributions at various long-term annealing were studied by Kumar et al.[9]. These authors observed very different partitioning of Mo, Cr, and Ni behavior in different precipitation types of σ phase (precipitation rims at high temperatures versus lamellar, "pseudo-eutectoid" formations at lower temperatures) depending on aging temperature and different interfaces.

Magnabosco and co-workers[13–16] used DICTRA[8] to study the precipitation of σ phase in duplex steels. By using different geometrical model setups (spherical, linear) for the position of the interface they could reproduce their experimental data[16] of the evolution of σ phase fraction at different aging times and proposed that σ phase formation would be controlled by nucleation and growth at low temperature aging, whereas diffusion would govern its formation at high temperatures.[14] By this Magnabosco et al.[13–16] offered an alternative formation mechanism to the usually given eutectoid mechanism. Their finding is in agreement with our previous thermodynamic study,[4] which confirmed that direct eutectoid reaction for σ phase formation in the hyper duplex system represents a non-equilibrium state. Moreover, we proposed in a previous kinetic simulation study[2] the requirement of Mo enrichment for the appropriate time-temperature-precipitation (TTP) behavior of σ phase.[5] This approach is to date however limited to one alloy matrix in the employed Mean-Field simulation with MatCalc.[17] Indeed, the formation of σ phase within one steel matrix phase, α, has also been observed in duplex steels.[10] However, since the hyper duplex material is subjected to considerable element partitioning between the two alloy matrix phases, α and γ, the Mean-Field approach within MatCalc can only picture part of the complete formation mechanism of σ phase. In DICTRA, blocks of different matrix phases, with and without an interphase, representing a heterogeneous precipitate, and their diffusive inter-relations, can be realized.

3 Materials and Methods

a) Computer simulation

Computational thermokinetics tools based on the Calphad approach[18] have been shown to provide consistent data for predictive thermokinetic precipitation simulation of intermetallic phases in materials science.[2,14] In the present work, DICTRA[8] is used for the study of α/γ, α/σ/γ, α/σ/α and γ/σ/γ interfaces at different holding temperatures in order to understand the mechanisms of formation of heterogeneous σ phase in hyper duplex steels. The results of DICTRA are based on the adapted thermodynamic and mobility steel databases mc_fe_v2.012 [https://www.matcalc.at/index.php/databases/open-databases] used for the Mean-Field calculations.[17]

DICTRA is based on the numerical solution of the diffusion equation in multicomponent systems and on the thermodynamic Calphad-modeled chemical potentials.[19] The moving boundary model used for the present work assumes local equilibrium across the phase interface. Equilibrium is defined by the minimum Gibbs energy surface of the phases from the thermodynamic database. The diffusional flux of elements follows Fick's law, as derived from the assessed diffusivities of elements stored in the diffusion mobility database. The rate of phase transformation is controlled by the transport of elements, and it is assumed that there is no difference in chemical potential between the two matrix phases. The values of chemical potentials are determined by the mass balance condition.

The studied hyper duplex steel has the same composition as given by Keplinger et al.[6] It is given in Table 1.

The calculated phase equilibria between α, σ, and γ of the studied system from the thermodynamic database developed for duplex σ phase materials[4] are given in Fig. 1.

Table 1. Chemical composition of the hyper duplex material used in the present study (in wt.%)

C	Mn	Si	Cr	Ni	Mo	Cu	N	Fe
0.005	2.9	0.2	26.3	6.9	4.6	0.2	0.37	Bal.

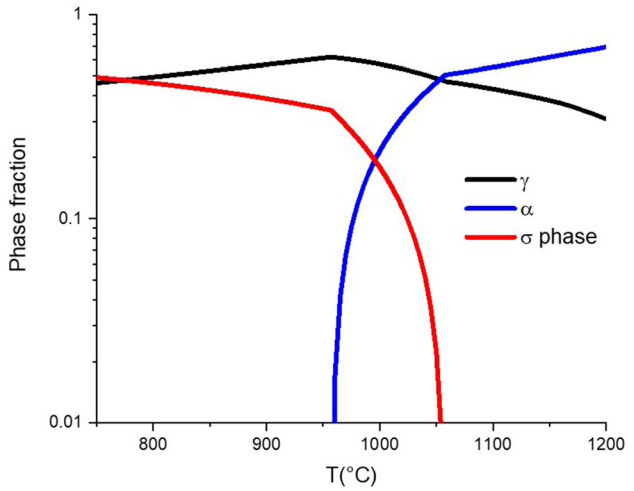

Fig. 1. Phase stability of the hyper duplex steel between 750 and 1200 °C

- **Simulation setup**

The rate of transformation at the interface of the matrix phases and early stage precipitation of σ phase is studied by DICTRA simulation. A planar geometry, representing a multilayered duplex microstructure, is used for the modeling of the moving boundary model.[19] The microstructure of a hyper duplex stainless steel is composed by the two steel matrix phases ferrite and austenite with an approximated fraction of 50/50 (mol.%). We consider a simulation cell dimension of 20 μm, and a start temperature of 1100 °C. This represents the temperature of initial solid solution treatment before quenching and aging, where computed equilibrium phase fractions are 52 % for ferrite and 48 % for austenite (Fig. 1). Accordingly, α domain has a size of 10.4 μm, and γ is 9.6 μm. Each domain contains 50 grid points. The σ phase is placed between the two-matrix domains with a size according to its equilibrium fraction of 9.4×10^{-4} μm or within one domain, i.e. in α/α or in γ/γ. For the simulation within one domain (i.e. ferrite or austenite), the total size is kept to 20 μm and σ phase is placed in the middle as the precipitate phase with the size given above.

As the computational effort for DICTRA to find the local kinetic properties is quite demanding and prone to numerical difficulties in multi-component systems, we restrict the moving boundary simulation to the four main elements Cr, Mo, Ni, and Fe involved in the precipitation of σ phase. Additionally, N is included in the calculation of elemental partitioning between α and γ at T = 1100 °C, but not in the DICTRA simulation. This conserves the duplex phase balance (i.e. 50:50 of α and γ, respectively). This method has been used earlier by Magnabosco et al.[15] for the same reason. The composition of α and γ at T = 1100 °C as calculated from the material Fe-26.3Cr-4.6Mo-6.9Ni-0.37N is given in Table 2.

Table 2. Composition (wt.%) of α and γ as obtained from the thermodynamic calculation at T = 1100 °C

	Ferrite (α)	Austenite (γ)
Cr	27.92	24.5
Mo	5.90	3.19
Ni	5.06	8.96
Fe	Bal.	Bal.

The evaluated chemical composition (Table 2) is used as the starting condition for the DICTRA simulation. We determine the embryonic σ phase nucleus, by assuming that the initial σ phase composition equals the composition of ferrite as nucleation is not possible with DICTRA. This assumption is reasonable since in principle the same elements stabilize the ferrite and σ phase. A scheme of the different studied domain setups is given in Fig. 2. Different annealing temperatures from 850 to 950 °C are used for t = 2000 s, thus including the nose temperature at T = 900 °C, where the rate of precipitation is maximal. The overall block size used for the simulation is 20 μm, and each sub-block (i.e. α and γ) size is set as given by the ratio between the phases calculated previously.

b) Aging experiments

The alloys were machined into cylinders with 4 mm diameter and 10 mm height and heat treated in a Bähr 805A/D dilatometer. Samples were heated to 1100 °C with a heating rate of 25 °C/s and held for 5 min, then rapidly cooled with a cooling rate of 50 °C/s to aging temperatures of 850, 900, 950 and 1000 °C and held for 25, 30, 50, and 75 s, and subsequently quenched to room temperature (with a cooling rate of 75 °C/s) under vacuum condition. The microstructures and chemical composition of phases were investigated by SEM/EDX using a Zeiss Sigma 500 VP SEM equipped with an EDAX OCTANE elect system.

4 Results and Discussion

1) Studying σ phase formation at three interface types at T = 900 °C

The different interfaces are studied individually for T = 900 °C which also represent heterogeneous sites for

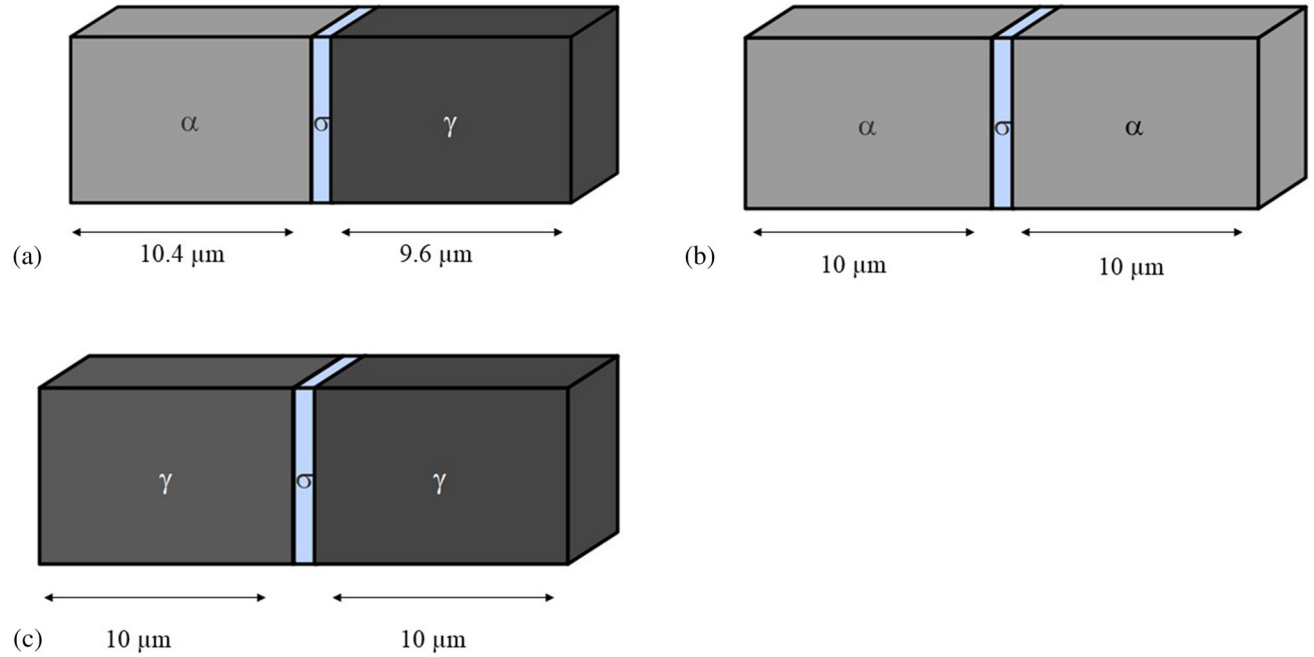

Fig. 2. Scheme of different simulation setups chosen for the DICTRA simulation with the different interfaces studied in the present work (**a**) α/σ/γ, (**b**) α/σ/α and (**c**) γ/σ/γ

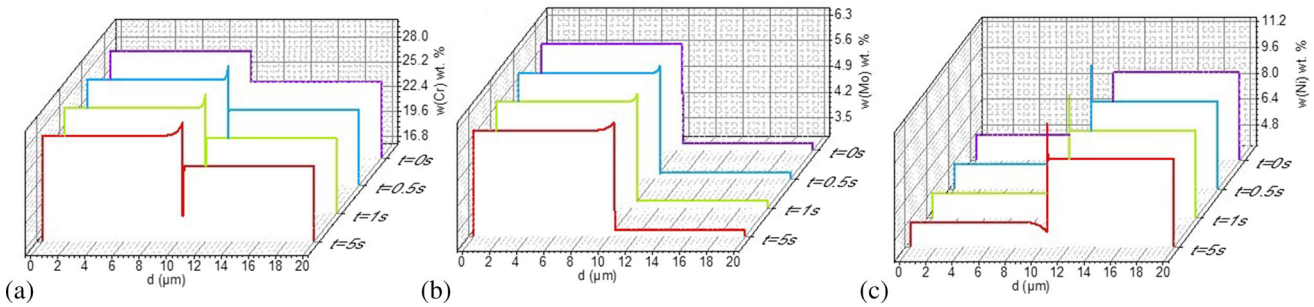

Fig. 3. Concentration profiles at T = 900 °C of (**a**) Cr, (**b**) Mo, and (**c**) Ni at the interface between α and γ as function of aging time

the precipitation of σ phase. These are the interfaces between α/γ, α/α and γ/γ. Additionally, the interface of the duplex structure α/γ is studied without the precipitate phase to better understand the pure matrix alloy pre-condition for precipitation.

a) Pure α/γ interface

At first, the results of the simulation of concentration profiles of the α/γ interface without consideration of σ phase are evaluated, as shown in Fig. 3, to measure of the element partitioning without precipitation of secondary phases.

During aging, the interface migration is controlled by mass balance from the flux of elements diffusing from one phase to another. The motion of the phases is associated with a strong partitioning of the elements (Fig. 3), which is the essence of a moving boundary. This partitioning is related to the previous solution annealing (T = 1100 °C) where the concentration of elements in both phases is different from their equilibrium composition at the considered aging temperature of 900 °C, and thus the elements get redistributed to reach the thermodynamic equilibrium state. The redistribution of the elements is evident even in absence of σ phase, as seen by a small variation of the phase fraction during aging in in-situ synchrotron investigations.[7] Without any other phase nucleation, Cr, Mo, and Ni accumulate at the interface, and boundaries move. At the same time, the elements prefer to stay in the phase where they are most preferred, i.e. Cr, Mo in α, and Ni in γ.

b) α/σ phase/γ

To study the early stage of the precipitation of σ phase, we now introduce a thin layer (i.e. 9×10^{-4} μm) of σ phase between the two alloy phases (α and γ) with all sizes

of phases respective to their equilibrium fraction. The resulting elemental concentrations profiles are given in Fig. 4.

Shortly after the start of the DICTRA simulation (t = 0.5 s), there is a strong accumulation of the elements at the interface between α and γ. This segregation of elements promotes σ phase formation, which thermodynamically prefers a large Cr and Mo solubility. Strikingly, at the interface σ/γ, a high accumulation of Mo up to 25 wt.% and Cr up to 35 wt.% is predicted (after 10 s), which shows the tremendous role of Cr and Mo in the pre-nucleation stage of σ phase and confirms earlier kinetic simulation findings.[2] It should be noted that there is no diffusion coefficient set for σ phase, but just for the diffusion of elements in the steel matrix phases, and the growth and composition change of σ phase in the present work is driven by the thermodynamic potentials and the diffusion in the steel matrix.

As postulated for the duplex steels,[10] the formation of σ is diffusion controlled, and the simulated diffusion of the elements at t = 1 s is given in Fig. 5 overlapping with their concentration profile.

The diffusion of elements, Cr, Mo, and Ni is intrinsically about 100 times faster in α with body-centered cubic (bcc) crystal structure than in face-centered cubic (fcc) γ, as shown in Fig. 6, extracted from the diffusion mobility database mc_fe.ddb. Still, the atoms diffuse in α as well as in γ, but they get "trapped" at the interface. This induces their segregation and a suitable driving force for the nucleation of σ phase. As Ni is a γ former, it will have the tendency to stay in the phase instead of diffusing into the evolving α, thus the amount of Ni at the interface σ/γ is limited compared to the α forming elements Cr and Mo. Both Cr and Mo, by contrast, will strongly diffuse from γ to α and within α, and a considerable fraction will accumulate and segregate at the interface σ/γ. The nucleation of σ phase is then strongly supported by this local supersaturation of elements, which was already indicated by Da Fonseca et al.[20] for duplex steels. Since σ phase tends to dissolve even higher amounts of Cr and Mo levels as compared to α, it consumes the latter during its growth and coarsening. The remaining high level of less soluble Ni in σ phase aids the precipitation of secondary austenite (γ_2). The precipitation between α/γ is considered as the Partitioning/Feeding interface.

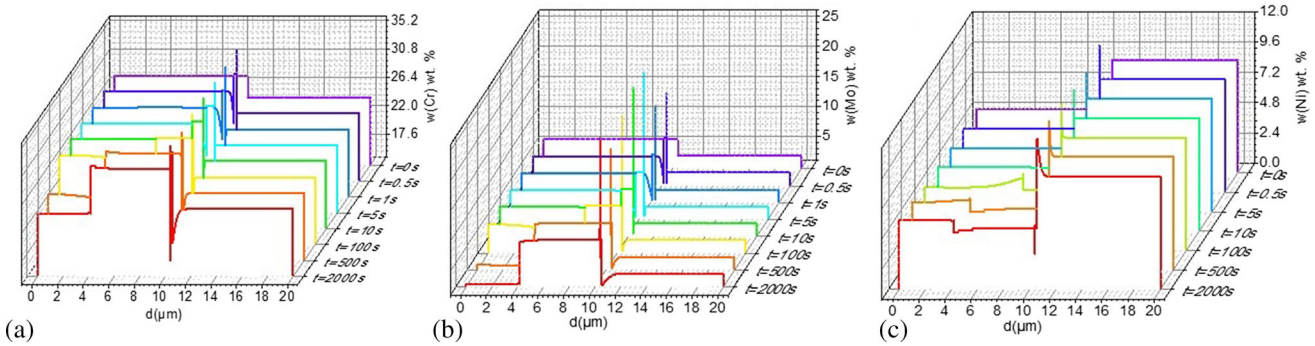

Fig. 4. Elemental distribution at T = 900 °C (**a**) Cr, (**b**) Mo and (**c**) Ni over time between the ferrite (left block), σ phase (center), and austenite (right block)

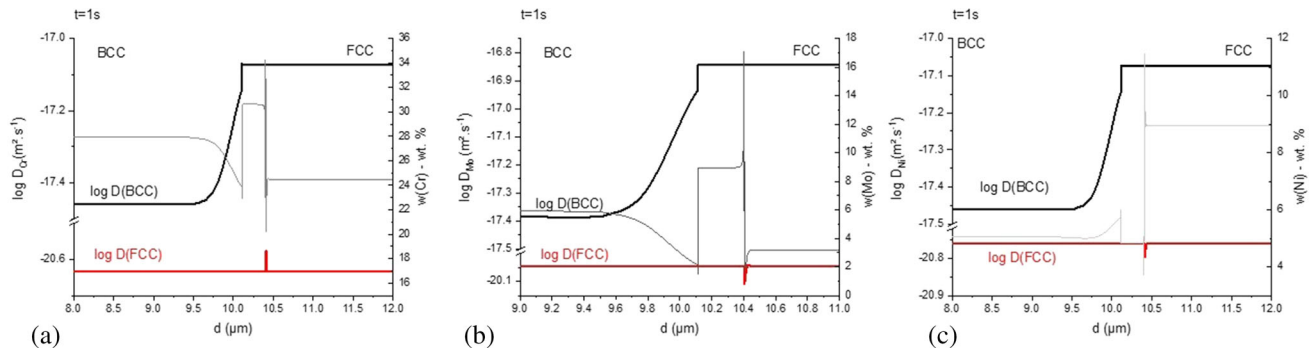

Fig. 5. Diffusion of elements at T = 900 °C and t = 1s for the different elements (**a**) Cr, (**b**) Mo and (**c**) Ni in both matrix overlapping the chemical composition. Ferrite (left block), σ phase (center), and austenite (right block)

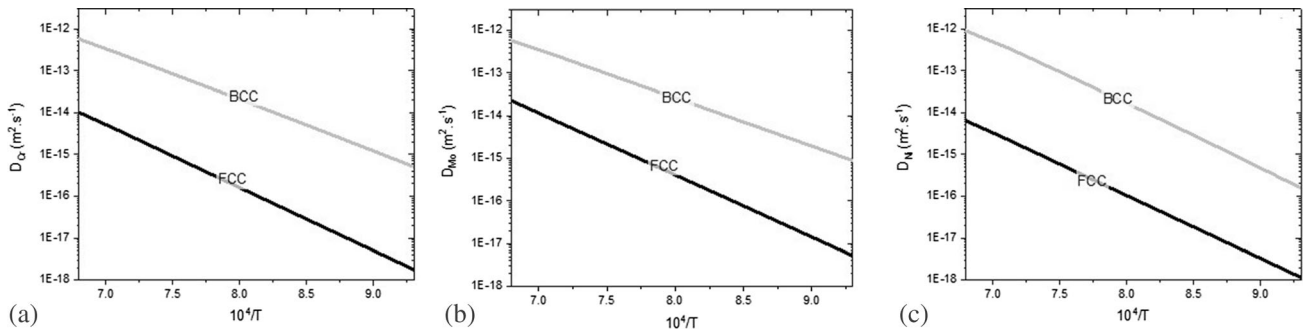

Fig. 6. Diffusion of the elements (**a**) Cr, (**b**) Mo and (**c**) Ni in the fcc (austenite) and bcc (ferrite) phases according to the mobility database mc_fe.ddb

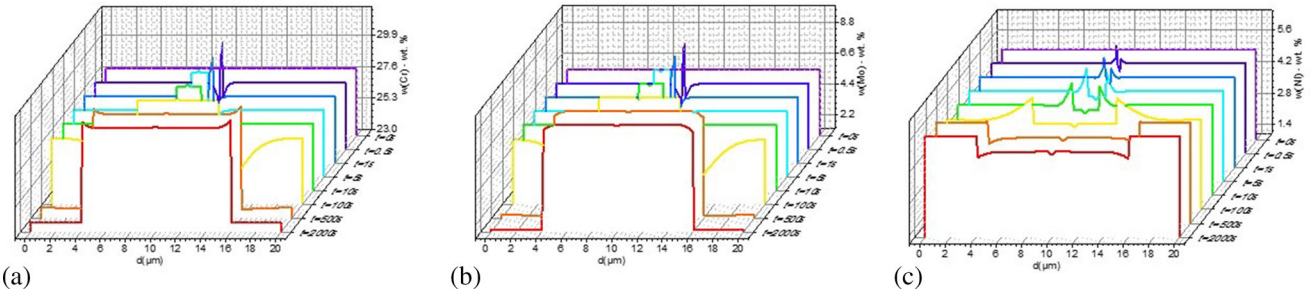

Fig. 7. Elemental concentration over time during aging at $T = 900$ °C at the α/α interface (**a**) Cr, (**b**) Mo and (**c**) Ni

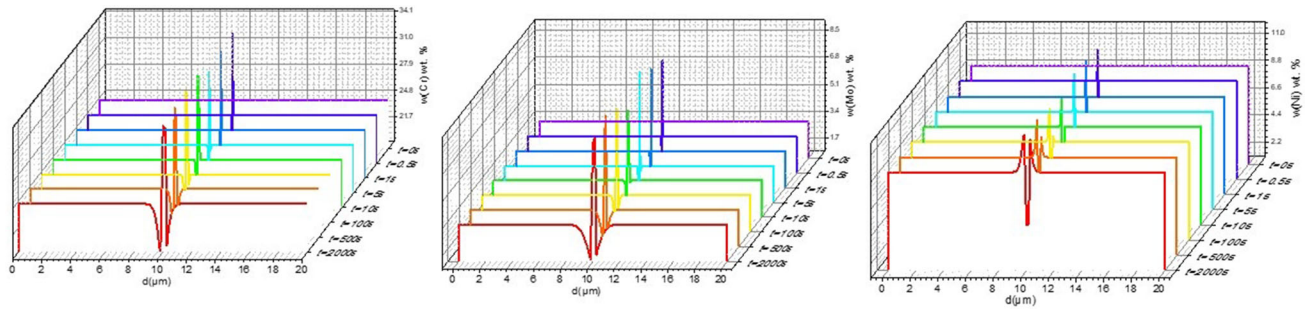

Fig. 8. Elemental concentration over time during aging at $T = 900$ °C at the γ/γ interface (**a**) Cr, (**b**) Mo and (**c**) Ni

c) α/σ phase/α

Now we investigate the interface α/α and the growth of σ during aging by tracking the chemical composition at different times (Fig. 7).

As previously, without γ, but providing the favorable elements to σ phase to the interface due to partitioning and their accumulation at the interface, promoting grain boundary (GB) segregation of elements such as Mo and Cr, σ phase precipitates. This case represents the situation within α phase regions in the material away from austenite. It is to be noted that the "slight" asymmetry of the elemental concentration at $t = 0.5$ and $t = 1$ s is due to numerical error and thus must not be interpreted. Diffusion of elements within α promotes the supersaturation of elements at the grain boundaries and thus provides a suitable driving force for the precipitation of σ phase. This phenomenon has already been found in our previous study.[2] The formation of σ phase within α has also been observed experimentally in duplex steels.[10] At the interface between σ phase and α, Ni tends to enrich, as it is not strongly dissolved in σ phase. However, Ni subsequently participates in the formation of secondary austenite γ_2 along the α/σ interface, which is not considered in the present simulation. The growth of σ phase in this domain is considered as the Segregating Interface fed by the fast mobility of elements in bcc which is finally consumed.

d) γ/σ phase/γ

As for the three other types of interfaces, there is the migration of the elements toward the interface (Fig. 8),

accumulating there. In principle, the resulting increased concentration of elements can lead to σ phase formation, nevertheless due to the slow diffusivity of elements in austenite, this site is not very favorable for the σ phase precipitation. While Zhang et al.[5] suggested from their microstructure analysis that there is precipitation of σ phase within purely austenitic regions, our investigations[7,9] did not confirm this at the early stage of precipitation. The present computation also suggests that the austenite grain boundary is unlikely to serve as a nucleation site for σ phase in hyper duplex steels due to the slow diffusivity and unfavorable driving force compared to the precipitation within the α regions and the α/γ boundaries. Thus, σ phase nuclei do not continue to grow from the austenite grain boundary, in contrast to the two other types of interface, and the role of γ/γ interface for the evolution of σ phase can be considered as negligible in hyper duplex steel.

2) Simulated σ phase fractions

The simulated total volume share depending on which interface σ phase precipitates is plotted as a function of time in Fig. 9 at T = 900 °C.

Clearly, the kinetically most favorable interface at T = 900 °C for precipitation of σ is the α/α. This is consistent with the "alike" elements for α and σ phase (i.e. Cr and Mo), *and* the fast diffusivity of elements. While σ phase nucleates, grows, and coarsens, the α phase is consumed. Whereas experimentally α would eventually be completely consumed, the simulation shows a minimum of ∼ 20 % ferrite remaining in equilibrium. This is due to the simplification in the DICTRA simulation where we need to choose only one type of interface at once, whereas experimentally, σ precipitation concurrently happens within α and at α/γ grain boundaries. Moreover, we neglect

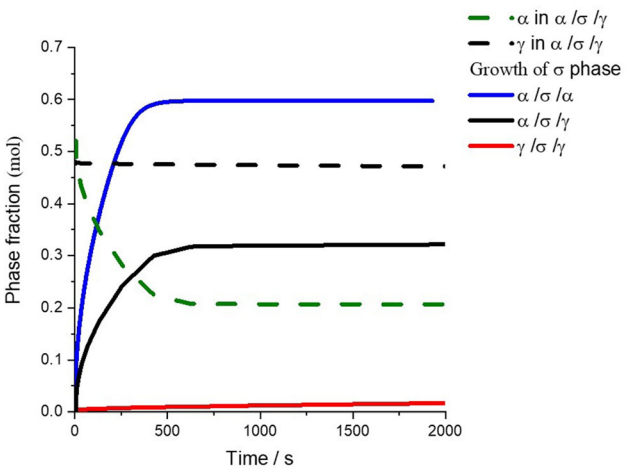

Fig. 9. Predicted evolution of σ phase amount during precipitation at T = 900 °C at different interfaces and total phase fraction of α and γ during σ phase precipitation in α/σ/γ

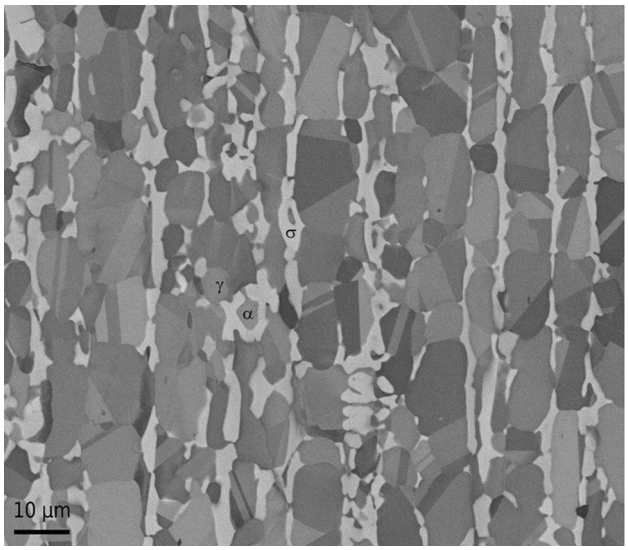

Fig. 11. Microstructure of "rim" σ phase decorating the grain boundary α/γ at T = 1000 °C for 6 h

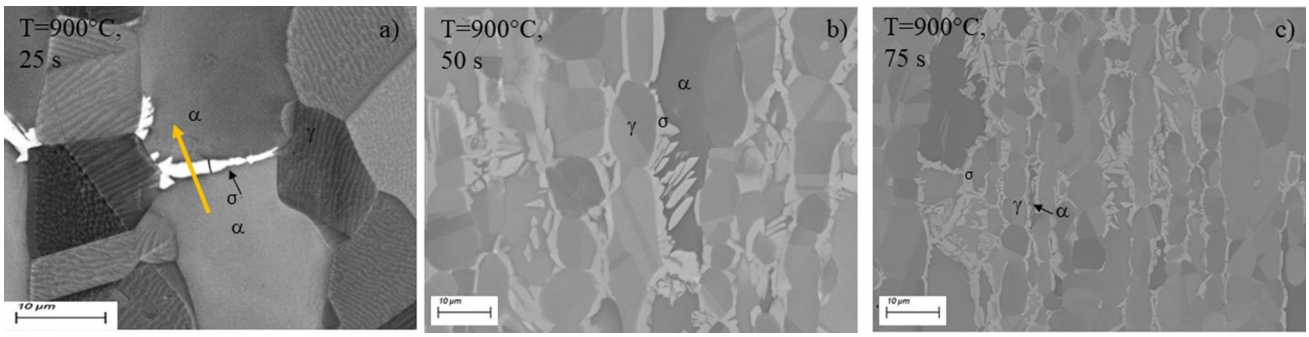

Fig. 10. Microstructure evolution of σ phase during short time annealing at T = 900 °C, (**a**) t = 25 s (yellow arrow representing line-scan analysis presented in Fig. 11), (**b**) 50 s and (**c**) 75 s

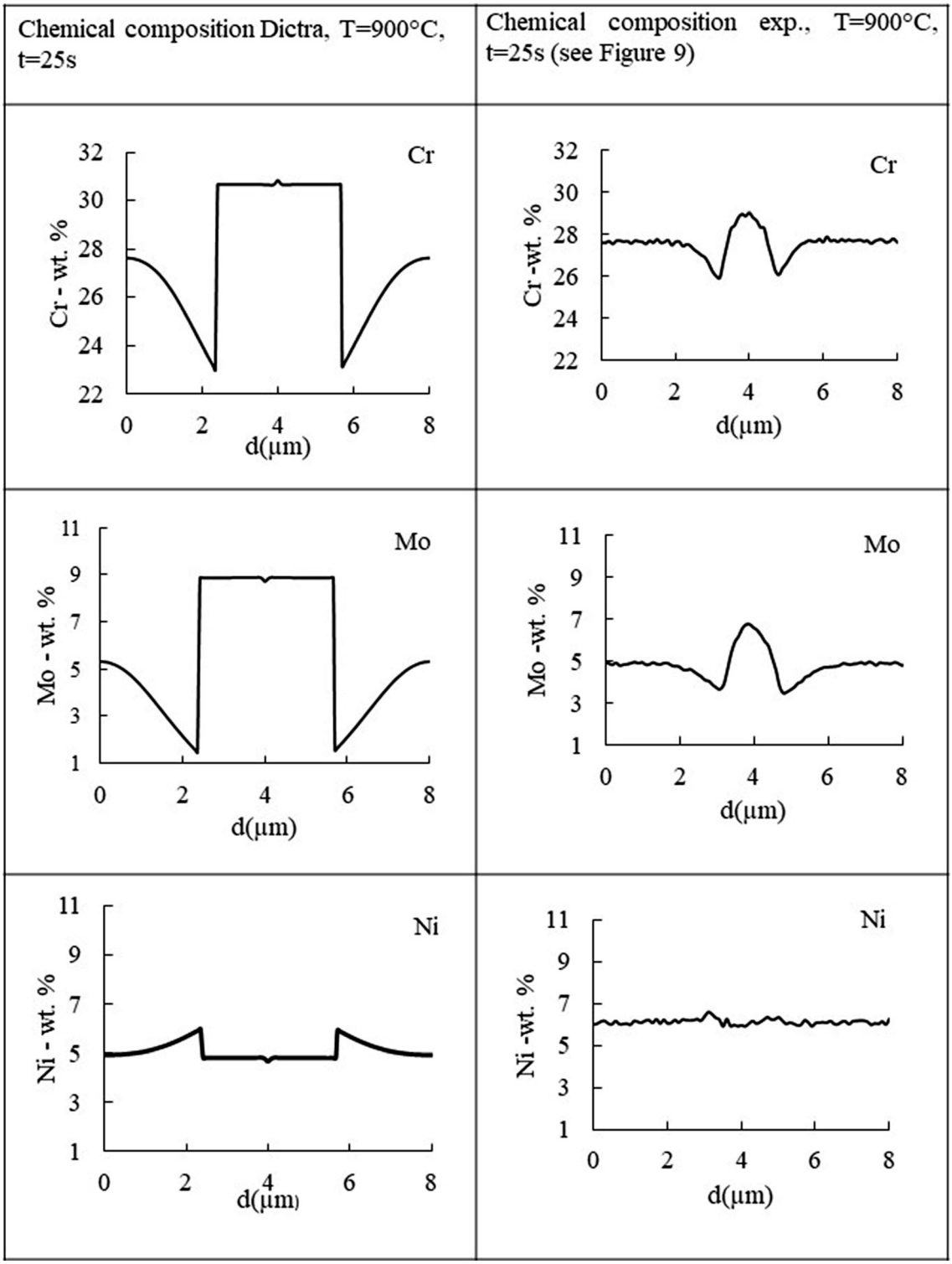

Fig. 12. Comparison between computed chemical composition and EDX measurements at T = 900 °C for 25 s within α/σ/α interface

the precipitation of secondary austenite γ_2 in the simulation, which affects the later stages of the hyper duplex microstructure evolution.

3) Correlation of simulation results to observed microstructures

As demonstrated by the study of α/γ and α/α interfaces (Figs. 4 and 7), the accumulation of elements (i.e. GB

segregation) at these interfaces strongly promotes the growth of σ phase. This is visible in the microstructure analysis of samples aged at T = 900 °C, where σ phase is first precipitating at α/α interfaces and then decorates α/γ grain boundaries (see microstructure evolution in Fig. 10). The growth of the precipitates follows then two different mechanisms as already demonstrated experimentally,[7] first, and at lower temperatures (i.e. $T \leq$ 950 °C) a short-range reaction-driven lamellar form appears within the ferrite region (see Fig. 10). The interface boundaries α/α are continuously enriched by the elements forming α which have an affinity for σ, i.e. elements Cr and Mo.

The second mechanism of growth is long-range bulk diffusion controlled and results in a cellular/rims form of σ phase being observed at the grain boundary of α/γ. Such a microstructure type is observed at higher temperatures, see Fig. 11 for the case of an annealing temperature of T = 1000 °C (for 6 h).

4.1 Phase Chemistry Considerations of σ Phase

Compositional trends of Cr and Mo: The computer simulation of DICTRA allows us to trace the evolution of the chemical composition of σ phase as function of time for different interfaces. Initially, the chemical composition is given as equilibrium at T = 1100 °C and evolves toward the equilibrium value of the aging temperatures. The first precipitated σ phase particles contain a large amount of Cr and Mo according to the simulation. The formation of σ phase also creates a depletion zone for these two elements at the interfaces to the matrix phases. This phenomenon can also be observed experimentally. In Fig. 12, which shows the measured chemical composition at the α/α interface by EDX in a sample annealed for 25 s at 900 °C. The computer simulation and experimental work provide consistent chemical compositional trends.

The compositional trend of Ni: Experimentally, Ni concentration remain ∼ 6 wt.% over the whole line-scan from α to σ and from σ to α while computationally there is a slight increase of Ni concentration at the interface by about 1 wt. %. The difference is due to the experimental detection limit due to the small composition change and the size of the interface.

4) Thermal evolution of σ phase fraction

To evaluate the effect of different aging temperatures, α/σ phase/γ interface simulation was used and the growth of σ phase at different temperatures, T = 850 °C, T = 950 °C, and T = 1000 °C, was evaluated as previously. The resulting phase fractions of σ phase are compared to experimental data (Fig. 13) from Schuster et al.[7] (dashed lines).

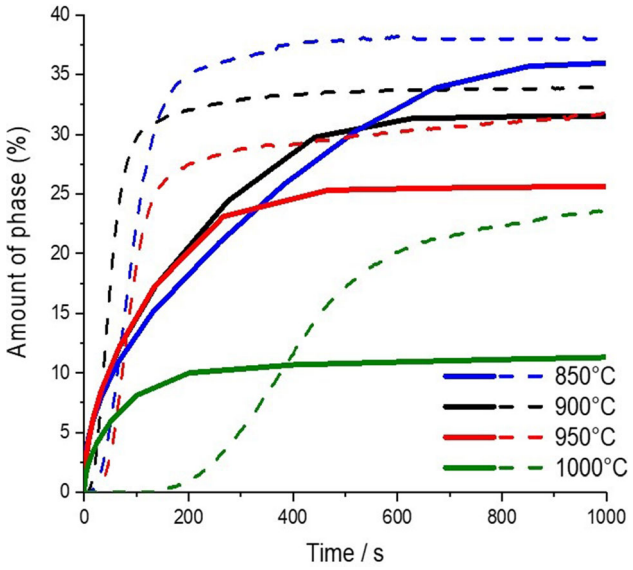

Fig. 13. Calculated phase fraction of σ precipitated at interface α/γ at T = 850, 900, and 950 °C (full lines) compared to experimental data [7] (dashed lines)

Note that the calculated phase fraction is restricted to one interface, whereas experimentally the precipitation can occur preferably in two types of interfaces (bear in mind that the γ/γ interface is not favorable). Nevertheless, the calculation can reproduce the same trend as the experiments, i.e. T = 900 °C is the temperature with the fastest σ phase formation.

5) Element segregation at the α/σ/γ interface at different temperatures

The elemental distribution at α/σ/γ interface for different aging temperatures is compared for the Cr, Mo, and Ni (Fig. 14) after a very short time of t = 1 s. While the segregation of Cr at σ/γ interface at the start of σ phase nucleation is about the same for all studied temperatures, which is indicated by increased Cr concentration of ∼ 34 wt.% Cr compared to 26.3 wt.% for the initial material composition, the segregation of Mo is the highest for T = 900 °C representing the nose temperature. Ni follows the opposite tendency of Mo, with the enrichment of Ni at the γ side and a Ni-depleted zone when Mo is highly enriched, consistent with the dissolution of Ni in secondary austenite.

The comparison between the different annealing temperatures indicates the peculiar role of Mo as the source for the incubation of σ phase due to its strong segregation at σ/γ interface.

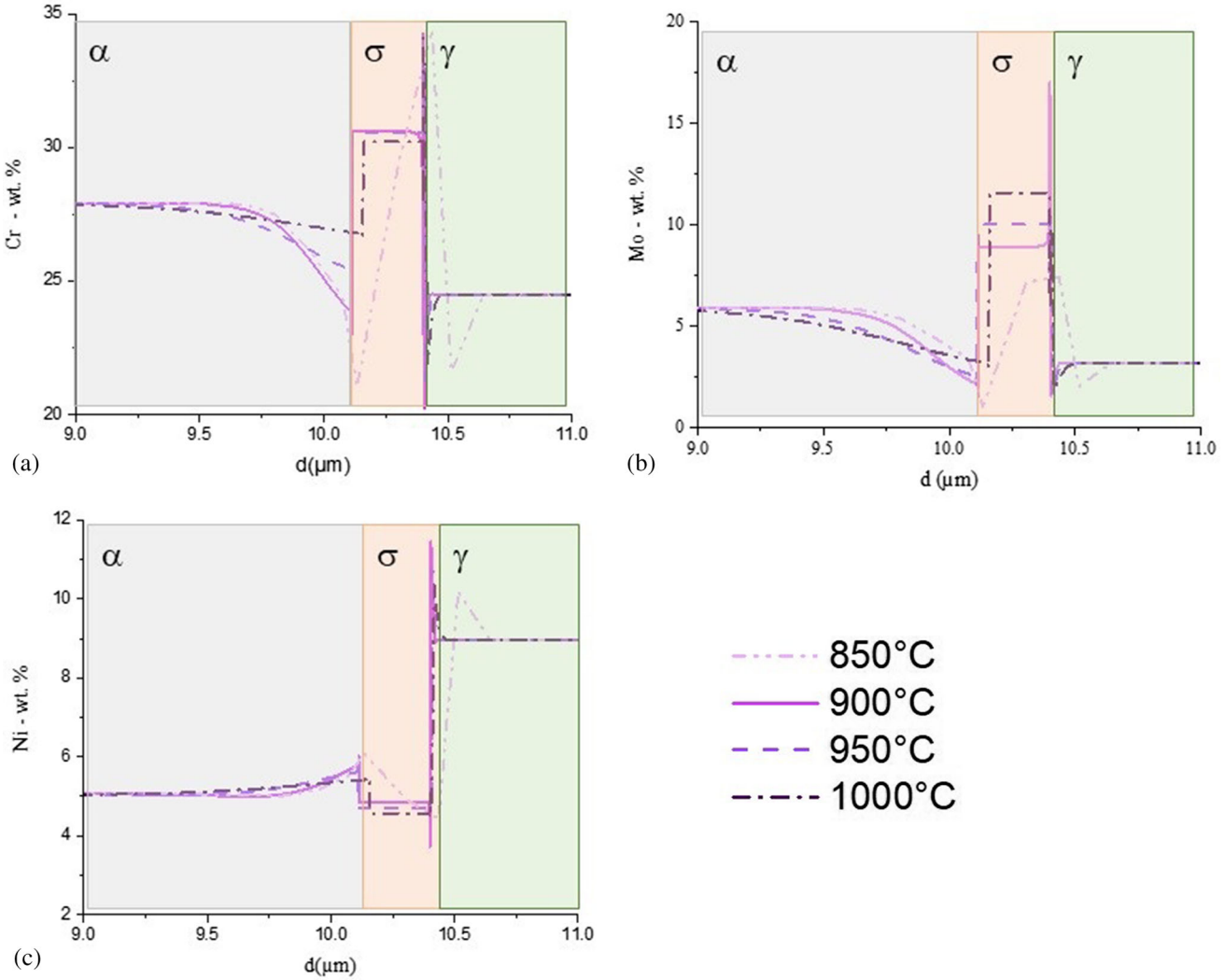

Fig. 14. Comparison of interface α/σ/γ evolution at t = 1 s at different annealing temperatures for (**a**) Cr, (**b**) Mo, and (**c**) Ni

6) Proposed mechanisms of σ phase precipitation in HDSS

Based on our previous experiments[7,9] and the present results, we propose the following parameters, which govern the formation of σ phase in high-alloyed duplex steels: Mo and its fast mobility plays a decisive role during the moving boundaries of the duplex structure, leading to its enrichment at the grain boundary, and making the grain boundary (α/α and α/γ) to become the "ideal" nucleation site for σ phase. Experimentally, the extent of the similar role of Cr cannot be resolved, whereas the present simulation also indicates the similarity with Mo, in terms of diffusivity and preference as σ phase former.

The growth of σ phase depends on the temperature and on the thermodynamic stability (and the related chemical driving force) of the phase. At high temperatures (i.e. T = 1000 °C), α is thermodynamically stable, and σ phase grows mostly along α/γ interface due to the re-partitioning of elements and associated with the most favorable positions of enriched Mo, and its growth is controlled by diffusion. Schuster et al.[7] (see Fig. 10 of the original paper) also observed this mechanism experimentally. On the other hand, at lower temperatures, of $T \leqslant T_{\text{nose}}$, the nucleation and growth of σ phase is interface and short-range reaction-diffusion controlled. Ferrite being metastable at these temperatures provides the most suitable and probable nucleation site/replacement site for σ phase.

From combined interpretation of the simulated kinetics of the present work and our previous in-situ XRD measurements[7] we can explain the observed microstructures in connection to σ phase. Roughly, the formation reaction of σ phase can be written α ➔ σ + γ, but it is convenient to elucidate the different steps of the formation of σ phase in more detail. Thermodynamically speaking the formation of σ phase follows the present mechanism: α ➔ [α + γ] ➔

$[\alpha + \gamma + \sigma] \rightarrow \sigma + \gamma$ and kinetically the path can be written $\alpha \rightarrow [\alpha + \sigma] \rightarrow [\alpha + \gamma + \gamma_2 + \sigma] \rightarrow \gamma + \gamma_2 + \sigma$, with $[\alpha + \sigma]$ forming at the grain boundary α/α (with a lamellar microstructure) and $[\alpha + \gamma + \gamma_2 + \sigma]$ occurring at the boundary α/γ and forming a cellular microstructure ("eutectoid –like pseudo-eutectoid microstructure").

5 Summary and Conclusion

It can be concluded from DICTRA simulation and experimental characterization[5,7,9] that for σ precipitation two of the three different interface types are strongly preferred, which are highly dependent on the Mo diffusion dynamics:

- $\alpha/\sigma/\alpha$ interface: Enrichment of Mo and Cr due to fast mobility in α and a precipitate-free zone at the interface σ/α (except for Ni which is a γ former). It can be considered as the Segregating Interface and is the most favorable site for σ phase precipitation. The mechanism of σ phase formation is diffusion controlled.
- $\alpha/\sigma/\gamma$ interface: Accumulation of Mo and Cr at the interface between α and γ (fed by α until complete consumption and by element partitioning from γ). It is a Partitioning/Feeding interface, the nucleation of new σ precipitate stops when there is not enough elemental supply for partitioning left and the ferrite is consumed. The σ phase continues to grow along secondary austenite.
- $\gamma/\sigma/\gamma$ interface: Enrichment of Mo and Cr at the interface due to aversion by γ and particle-free zone at the interface. This site is not favorable due to slow diffusivity and can be considered negligible.

Acknowledgments The financial support from the Austrian Federal Ministry for Digital and Economic Affairs and the National Foundation for Research, Technology, and Development are gratefully acknowledged. This research was funded by Christian Doppler Forschungsgesellschaft in the framework of the CD-Laboratory of Interfaces and Precipitation Engineering. The authors acknowledge Open access Funding by TU Wien.

Funding Open access funding provided by TU Wien (TUW).

References

1. G. Chail, and P. Kangas, Super and Hyper Duplex Stainless Steels: Structures, Properties and Applications, *Procedia Struct. Integr.*, 2016, **2**, p 1755–1762. https://doi.org/10.1016/j.prostr.2016.06.221
2. A. Jacob, and E. Povoden-Karadeniz, Predictive Computations of Intermetallic σ Phase Evolution in Duplex Steel. II) Thermo-Kinetic Simulation in Duplex and Hyper Duplex Stainless Steels, *Calphad*, 2020, **71**, p 101998. https://doi.org/10.1016/j.calphad.2020.101810
3. A. Jacob, E. Povoden-Karadeniz, and E. Kozeschnik, Revised Thermodynamic Description of the Fe-Cr System Based on an Improved Sublattice Model of the σ Phase, *Calphad*, 2018, **60**, p 16–28. https://doi.org/10.1016/j.calphad.2017.10.002
4. A. Jacob, and E. Povoden-Karadeniz, Predictive Computations of Intermetallic σ Phase Evolution in Duplex Steel. I) Thermodynamic Modeling of σ Phase in the Fe-Cr-Mn-Mo-Ni System, *Calphad*, 2020, **71**, p 101810. https://doi.org/10.1016/j.calphad.2020.101998
5. B. Zhang, Z. Jiang, H. Li, S. Zhang, H. Feng, and H. Li, Precipitation Behavior and Phase Transformation of Hyper Duplex Stainless Steel UNS S32707 at Nose Temperature, *Mater Charact*, 2017, **129**, p 31–39. https://doi.org/10.1016/j.matchar.2017.04.018
6. A. Keplinger, C. Martinez, M. Hausbauer, and M. Kapp, Early Stages of Deleterious Phases in Super-and Hyper Duplex Stainless Steel and Their Effect on Toughness ESSC DUPLEX 2019–10th, *Eur. Stainl. Steel Conf. Sci. Mark. 6th Eur Duplex Stainl. Steel Conf. Exhib.*, 2019, **165**, p 118–127. https://doi.org/10.1007/s00501-019-00936-4
7. R. Schuster, A. Keplinger, A. Jacob, J. Kreyca, L. Solyom, E. Maawad, and E. Povoden-Karadeniz, In-Situ XRD Investigation of σ Phase Precipitation Kinetics During Isothermal Holding in a Hyper Duplex Stainless Steel, *Mater Charact*, 2023, **2023**, 113124. https://doi.org/10.1016/j.matchar.2023.113124
8. J.O. Andersson, T. Helander, L. Höglund, P. Shi, and B. Sundman, Thermo-Calc & DICTRA, Computational Tools for Materials Science, *Calphad*, 2002, **26**, p 273–312. https://doi.org/10.1016/S0364-5916(02)00037-8
9. S. Kumar, S. Krisam, A. Jacob, F. Kiraly, A. Keplinger, R. Abart, and E. Povoden-Karadeniz, Microstructures and Elements Distributions in an Aged Hyper Duplex Stainless Steels and Corresponding Hardness Variation, *Under Revis. Mater. Des.*, 2020, **194**, p 108951.
10. J.W. Elmer, T.A. Palmer, and E.D. Specht, Direct Observations of Sigma Phase Formation in Duplex Stainless Steels Using In-Situ Synchrotron X-ray Diffraction, *Metall. Mater. Trans. A Phys. Metall. Mater. Sci.*, 2007, **38**, p 464–475. https://doi.org/10.1007/s11661-006-9076-3
11. M. Martins, and L.C. Casteletti, Sigma Phase Morphologies in Cast and Aged Super Duplex Stainless Steel, *Mater Charact*, 2009, **60**, p 792–795. https://doi.org/10.1016/j.matchar.2009.01.005
12. B. Zhang, H. Li, S. Zhang, Z. Jiang, Y. Lin, H. Feng, and H. Zhu, Effect of Nitrogen on Precipitation Behavior of Hyper Duplex Stainless Steel S32707, *Mater Charact*, 2021, **175**, 111096. https://doi.org/10.1016/j.matchar.2021.111096
13. R. Magnabosco, Kinetics of Sigma Phase Formation in a Duplex Stainless Steel 2. Experimental Procedure, *Mater. Res.*, 2009, **12**, p 321–327. https://doi.org/10.1590/S1516-14392009000300012
14. D.C. dos Santos, and R. Magnabosco, Kinetic Study to Predict Sigma Phase Formation in Duplex Stainless Steels, *Metall. Mater. Trans. A Phys. Metall. Mater. Sci.*, 2016, **47**, p 1554–1565. https://doi.org/10.1007/s11661-016-3323-z

15. R. Magnabosco, L. da Costa Morais, and D.C. dos Santos, Use of Composition Profiles Near Sigma Phase for Assessment of Localized Corrosion Resistance in a Duplex Stainless Steel, *Calphad Comput. Coupling Phase Diagr. Thermochem.*, 2019, **64**, p 126–130. https://doi.org/10.1016/j.calphad.2018.12.004
16. L.C. da Morais, and R. Magnabosco, Experimental Investigations and DICTRA® Simulation of Sigma Phase Formation in a Duplex Stainless Steel, *Calphad Comput. Coupling Phase Diagr. Thermochem.*, 2017, **58**, p 214–218. https://doi.org/10.1016/j.calphad.2017.07.006
17. E. Kozeschnik, Mean-Field Microstructure Kinetics Modeling, *Encycl. Mater. Met. Alloy.*, 2022, **4**, p 521–526. https://doi.org/10.1016/B978-0-12-819726-4.00055-7
18. H.L. Lukas, S.G. Fries, and B. Sundman, *Computational Thermodynamics the Calphad Method*. Cambridge University Press, Cambridge, 2007. https://doi.org/10.1017/CBO9780511804137
19. A. Borgenstam, A. Engstro, L. Ho Lund, and J.A. Ren, Basic and Applied Research: Section I DICTRA, a Tool for Simulation of Diffusional Transformations in Alloys, *J. Phase Equilib.*, 2000, **21**, p 269–280.
20. G.S. da Fonseca, P.S.N. Mendes, and A.C.M. Silva, Sigma Phase: Nucleation and Growth, *Metals (Basel)*, 2019. https://doi.org/10.3390/met9010034